

Hierarchical vs Degenerate 2HDM: The LHC Run 1 Legacy at the Onset of Run 2

G. C. Dorsch^{1,2}, S. J. Huber¹, K. Mimasu¹ and J. M. No¹

¹*Department of Physics and Astronomy, University of Sussex, BN1 9QH Brighton, United Kingdom and*

²*DESY, Notkestrasse 85, D-22607 Hamburg, Germany*

(Dated: January 19, 2016)

Current discussions of the allowed two-Higgs-doublet model (2HDM) parameter space after LHC Run 1 and the prospects for Run 2 are commonly phrased in the context of a quasi-degenerate spectrum for the new scalars. Here we discuss the generic situation of a 2HDM with a non-degenerate spectrum for the new scalars. This is highly motivated from a cosmological perspective since it naturally leads to a strongly first order electroweak phase transition that could explain the matter-antimatter asymmetry in the Universe. While constraints from measurements of Higgs signal strengths do not change, those from searches of new scalar states get modified dramatically once a non-degenerate spectrum is considered.

I. INTRODUCTION

While ongoing analyses by both ATLAS and CMS show that the properties of the Higgs particle at $m_h \sim 125$ GeV are close to those expected for the Standard Model (SM) Higgs boson h_{SM} [1, 2], the complete nature of the scalar sector responsible for electroweak (EW) symmetry-breaking remains to be determined. It is particularly interesting to ascertain whether the scalar sector consists of only one $\text{SU}(2)_L$ doublet or has a richer structure containing additional states. Addressing this question is a very important task for present and future studies at the Large Hadron Collider (LHC).

In this work we concentrate on models with two Higgs doublets (2HDM) (see [3] for a review), which appear in many extensions of the SM, such as the MSSM or scenarios of viable Electroweak Baryogenesis [4–8]. In recent years, the region of the parameter space for the 2HDM allowed by Higgs coupling measurements at ATLAS and CMS [9] has been widely studied in the literature [10–17]. Various works have also discussed the constraints coming from LHC searches for neutral and charged scalars A_0 , H_0 , H^\pm via $A_0 \rightarrow Zh$, $A_0/H_0 \rightarrow \tau\tau$, $A_0/H_0 \rightarrow \gamma\gamma$, $H_0 \rightarrow ZZ/WW$, $H_0 \rightarrow hh$, $H^\pm \rightarrow tb$ and $H^\pm \rightarrow \tau\nu$ (see *e.g.* [18, 19] for recent analyses). However, the interpretation of these constraints typically assumes that the new scalars can only decay into SM states, which requires H_0 , A_0 and H^\pm to be relatively close in mass (see however [28–30]). In the following we refer to this scenario as the *degenerate* 2HDM.

On the other hand, it has recently been shown [8] that sizable mass splittings between the 2HDM scalars (in particular a large $m_{A_0} - m_{H_0}$) favour a strong EW phase transition that could lead to baryogenesis. This provides an important physical motivation for a 2HDM scenario in which new decay channels for the heavier scalars are kinematically allowed (*e.g.* $A_0 \rightarrow ZH_0$), a situation which has so far been largely neglected in the literature. We refer to this scenario as the *hierarchical* 2HDM. It is the purpose of this work to fill this gap, providing a detailed discussion of the constraints on the 2HDM parameter space from 7 and 8 TeV LHC Run 1 data,

comparing the degenerate and hierarchical 2HDM scenarios. We will show that, besides significantly weakening the bounds from searches for these new scalars into SM states, the sizable mass splittings provide possibilities for novel searches (see *e.g.* [20]) which can yield complementary limits on the 2HDM parameter space. We assess the interplay between these searches, the standard searches for new scalars decaying directly into SM particles, and the measurement of 125 GeV Higgs signal strengths in constraining 2HDM scenarios. Furthermore, being at the onset of LHC Run 2, we go on to outline the upcoming prospects for direct searches of the neutral scalars H_0 , A_0 in the hierarchical 2HDM at the 13 TeV Run of LHC, through the discussion of benchmark plane scenarios.

After a review of the 2HDM in Section II, we discuss the measurements of Higgs signal strengths in the context of the 2HDM in Section III A. We then demonstrate the impact of the mass spectrum on LHC searches for A_0/H_0 in Sections III B and III C as well as briefly commenting on H^\pm searches in Section III D. In Section III E we go on to analyze the constraints that can be derived from the recent dedicated search of 2HDM neutral scalars with a sizable splitting by the CMS Collaboration [20], highlighting the strong complementarity with the Standard searches and analyzing the interplay between these and Higgs measurements discussed in Section III A. Finally, in Section IV we present benchmark plane scenarios for searches of these new scalars at LHC Run 2.

II. A (BRIEF) REVIEW OF THE 2HDM

In this section we discuss the aspects of the 2HDM relevant to our analysis, defining at the same time our notation. We consider a general 2HDM scalar potential with a softly broken \mathbb{Z}_2 symmetry in the absence of Charge-Parity (CP) violation, which reads

$$\begin{aligned}
 V(H_1, H_2) = & \mu_1^2 |H_1|^2 + \mu_2^2 |H_2|^2 - \mu^2 \left[H_1^\dagger H_2 + \text{h.c.} \right] \\
 & + \frac{\lambda_1}{2} |H_1|^4 + \frac{\lambda_2}{2} |H_2|^4 + \lambda_3 |H_1|^2 |H_2|^2 \quad (1) \\
 & + \lambda_4 \left| H_1^\dagger H_2 \right|^2 + \frac{\lambda_5}{2} \left[\left(H_1^\dagger H_2 \right)^2 + \text{h.c.} \right],
 \end{aligned}$$

where the two scalar $SU(2)_L$ doublets H_j ($j = 1, 2$) may be written as

$$H_j = \left(\phi_j^+, (v_j + h_j + i\eta_j)/\sqrt{2} \right)^T. \quad (2)$$

In addition to the 125 GeV Higgs state h , the scalar sector of a 2HDM includes another neutral CP-even scalar H_0 , a neutral CP-odd scalar A_0 and a charged scalar H^\pm . For most of this work, we assume that these new states are heavier than h (it is however possible, although more experimentally constrained, for either H_0 or A_0 to be lighter than $m_h = 125$ GeV, a possibility which has been explored recently in [21, 22]). Apart from m_h and $v = 246$ GeV, the scalar potential (1) may be parametrized in terms of the scalar masses m_{H_0} , m_{A_0} , m_{H^\pm} , the squared mass scale μ^2 and two angles β and α , the former being related to the ratio of vacuum expectation values (*vevs*) of the two scalar doublets, $v_{1,2}$, via $\tan\beta \equiv v_2/v_1$ (with $v_1^2 + v_2^2 = v^2$) and the latter parametrising the mixing between the CP-even states. The relation between the physical states h , H_0 , A_0 , H^\pm and the states h_j , η_j , ϕ_j^\pm is given by

$$\begin{aligned} H^\pm &= -s_\beta \phi_1^\pm + c_\beta \phi_2^\pm & A_0 &= -s_\beta \eta_1 + c_\beta \eta_2 \\ h &= -s_\alpha h_1 + c_\alpha h_2 & H_0 &= -c_\alpha h_1 - s_\alpha h_2 \end{aligned}$$

with $s_\beta, c_\beta, s_\alpha, c_\alpha \equiv \sin\beta, \cos\beta, \sin\alpha, \cos\alpha$, respectively. Regarding the couplings of the two doublets $H_{1,2}$ to fermions, the \mathbb{Z}_2 in (1), even when softly broken by μ^2 , may be used to forbid potentially dangerous tree-level flavour changing neutral currents (FCNCs) by requiring that each fermion type couple to one doublet only [23]. By convention, up-type quarks couple to H_2 . In Type I 2HDM all the other fermions also couple to H_2 , while for Type II down-type quarks and leptons couple to H_1 . There are two more possibilities (depending on the \mathbb{Z}_2 parity assignment for leptons with respect to down-type quarks), but we focus here on Types I and II, as they encode the relevant physics of 2HDMs with no tree-level FCNCs.

The parameters $t_\beta \equiv \tan\beta$ and $c_{\beta-\alpha} \equiv \cos(\beta - \alpha)$ control the strength of the couplings of h , H_0 , A_0 and H^\pm to gauge bosons and fermions. Focusing on the neutral scalars, we denote the couplings normalized to the SM values (of h_{SM}) by κ -factors (κ_V for gauge bosons, κ_u for up-type quarks, κ_d for down-type quarks, κ_ℓ for charged leptons), which read

$$\text{Type - I : } \begin{cases} \kappa_V^h = s_{\beta-\alpha} \\ \kappa_u^h = \kappa_d^h = \kappa_\ell^h = t_\beta^{-1} c_{\beta-\alpha} + s_{\beta-\alpha} \\ \kappa_V^{H_0} = -c_{\beta-\alpha} \\ \kappa_u^{H_0} = \kappa_d^{H_0} = \kappa_\ell^{H_0} = t_\beta^{-1} s_{\beta-\alpha} - c_{\beta-\alpha} \\ \kappa_u^{A_0} = -\kappa_d^{A_0} = -\kappa_\ell^{A_0} = t_\beta^{-1} \end{cases} \quad (3)$$

$$\text{Type - II : } \begin{cases} \kappa_V^h = s_{\beta-\alpha} \\ \kappa_u^h = t_\beta^{-1} c_{\beta-\alpha} + s_{\beta-\alpha} \\ \kappa_d^h = \kappa_\ell^h = s_{\beta-\alpha} - t_\beta c_{\beta-\alpha} \\ \kappa_V^{H_0} = -c_{\beta-\alpha} \\ \kappa_u^{H_0} = t_\beta^{-1} s_{\beta-\alpha} - c_{\beta-\alpha} \\ \kappa_d^{H_0} = \kappa_\ell^{H_0} = -t_\beta s_{\beta-\alpha} - c_{\beta-\alpha} \\ \kappa_u^{A_0} = t_\beta^{-1} \\ \kappa_d^{A_0} = \kappa_\ell^{A_0} = t_\beta \end{cases} \quad (4)$$

For $c_{\beta-\alpha} \rightarrow 0$, commonly referred to as the 2HDM *alignment* limit, h has SM-like couplings to gauge bosons and fermions ($\kappa_i^h \rightarrow 1$, yielding $h \rightarrow h_{\text{SM}}$), while the coupling $H_0 VV$ of H_0 to gauge bosons $V = W^\pm, Z$ vanishes ($\kappa_V^{H_0} \rightarrow 0$).

In order to obtain a viable 2HDM scenario, theoretical constraints from unitarity, perturbativity and stability/boundedness from below of the scalar potential (1) need to be satisfied. Tree-level stability of the potential $V(H_1, H_2)$ requires $\lambda_1 > 0$, $\lambda_2 > 0$, $\lambda_3 > -\sqrt{\lambda_1 \lambda_2}$, $\lambda_3 + \lambda_4 - |\lambda_5| > -\sqrt{\lambda_1 \lambda_2}$ (see *e.g.* [24]). At the same time, tree-level unitarity¹ imposes bounds on the size of various combinations of the quartic couplings λ_i [26], like $|\lambda_3 \pm \lambda_4| < 8\pi$, $|\lambda_3 \pm \lambda_5| < 8\pi$, $|\lambda_3 + 2\lambda_4 \pm 3\lambda_5| < 8\pi$ and $|\lambda_1 + \lambda_2 \pm \sqrt{(\lambda_1 - \lambda_2)^2 + 4\lambda_4^2}| < 16\pi$. Similar (although generically less stringent) bounds on λ_i may be obtained from perturbativity arguments. We may express λ_i in terms of the physical scalar masses, the mixing angles α , β and μ^2 :

$$\lambda_1 = \frac{1}{v^2 c_\beta^2} (-\mu^2 t_\beta + m_h^2 s_\alpha^2 + m_{H_0}^2 c_\alpha^2), \quad (5)$$

$$\lambda_2 = \frac{1}{v^2 s_\beta^2} (-\mu^2 t_\beta^{-1} + m_h^2 c_\alpha^2 + m_{H_0}^2 s_\alpha^2), \quad (6)$$

$$\lambda_3 = \frac{1}{v^2} \left[-\frac{2\mu^2}{s_{2\beta}} + 2m_{H^\pm}^2 + (m_{H_0}^2 - m_h^2) \frac{s_{2\alpha}}{s_{2\beta}} \right], \quad (7)$$

$$\lambda_4 = \frac{1}{v^2} \left(\frac{2\mu^2}{s_{2\beta}} + m_{A_0}^2 - 2m_{H^\pm}^2 \right), \quad (8)$$

$$\lambda_5 = \frac{1}{v^2} \left(\frac{2\mu^2}{s_{2\beta}} - m_{A_0}^2 \right). \quad (9)$$

As seen from (5-9), for a given set of values for m_{H_0} , m_{A_0} , m_{H^\pm} , t_β and $c_{\beta-\alpha}$, only a certain range for μ^2 is allowed by the combination of these theoretical constraints. In particular, $\lambda_{1,2} > 0$ directly imply an upper bound on μ^2 from (5)-(6). It is however possible that no value of μ^2 allows to satisfy all three theoretical requirements simultaneously, in which case such a set of values for the scalar masses and mixing angles would not be viable. If an allowed μ^2 range exists, the size of trilinear scalar couplings such as $\lambda_{H_0 h h}$ and $\lambda_{H_0 A_0 A_0}$ (which control the partial widths $\Gamma_{H_0 \rightarrow h h}$, $\Gamma_{H_0 \rightarrow A_0 A_0}$ when these decays are

¹ For a recent one-loop analysis, leading to slightly more stringent bounds, see [25].

kinematically allowed) or $\lambda_{hH^+H^-}$ (which controls the size of the charged scalar loop contribution to the $h \rightarrow \gamma\gamma$ decay amplitude, given by Δ_γ^\pm) depend on the value of μ^2 . Indeed, the trilinear couplings λ_{H_0hh} and $\lambda_{H_0A_0A_0}$ are given by

$$v\lambda_{H_0hh} = \frac{2c_{\beta-\alpha}}{s_{2\beta}} \left[\left(1 - 3\frac{s_{2\alpha}}{s_{2\beta}}\right) \mu^2 + (2m_h^2 + m_{H_0}^2) \frac{s_{2\alpha}}{2} \right] \quad (10)$$

$$v\lambda_{H_0A_0A_0} = 2 \left[c_{\beta-\alpha} (2m_{A_0}^2 + m_{H_0}^2) - 2 \left(s_{\beta-\alpha} \frac{c_{2\beta}}{s_{2\beta}} - c_{\beta-\alpha} \right) \left(m_{H_0}^2 - \frac{\mu^2}{s_\beta c_\beta} \right) \right] \quad (11)$$

Apart from vanishing in the alignment limit, if $s_{2\beta} - 3s_{2\alpha} \neq 0$, the coupling λ_{H_0hh} also vanishes for $\mu^2 = (2m_h^2 + m_{H_0}^2)(s_{2\alpha}s_{2\beta})/(6s_{2\alpha} - 2s_{2\beta})$, if such value of μ^2 lies within the allowed range. Similarly, in the alignment limit $\lambda_{H_0A_0A_0}$ vanishes for $t_\beta = 1$ or $\mu^2 = m_{H_0}^2 s_\beta c_\beta$. The trilinear coupling $\lambda_{hH^+H^-}$ reads

$$v\lambda_{hH^+H^-} = \left[s_{\beta-\alpha} (m_h^2 - 2m_{H^\pm}^2) - 2 \left(c_{\beta-\alpha} \frac{c_{2\beta}}{s_{2\beta}} + s_{\beta-\alpha} \right) \left(m_h^2 - \frac{\mu^2}{s_\beta c_\beta} \right) \right], \quad (12)$$

so that Δ_γ^\pm inherits a dependence on μ^2 and other 2HDM parameters besides $m_{H^\pm}^2$ through $\lambda_{hH^+H^-}$. These trilinear couplings illustrate the phenomenological impact of the soft \mathbb{Z}_2 -breaking parameter in the 2HDM, which will be analyzed in more detail in Section III.

III. HIERARCHICAL VS DEGENERATE 2HDM: THE LHC RUN 1 LEGACY

Let us now concentrate on the mass spectrum of the 2HDM. We first note that constraints from measurements of EW precision observables (EWPO), in particular of the T -parameter, generically require H^\pm to be relatively degenerate with either A_0 or H_0 [27]. From a phenomenological perspective we can then distinguish between a *degenerate* spectrum where all mass splittings among the new scalar states are small, $|m_{A_0} - m_{H_0}| \ll m_Z$, and a *hierarchical* spectrum for which the mass splitting among the new neutral scalars is sizable, $|m_{A_0} - m_{H_0}| \gtrsim m_Z$.

The main phenomenological feature of a hierarchical 2HDM spectrum is that the decays $\varphi_i \rightarrow \varphi_j V$, with $\varphi_{i,j} = H_0, A_0, H^\pm$ ($i \neq j$) and $V = W^\pm, Z$ become kinematically allowed and generically yield the dominant branching fraction, with the decays into SM states comparatively suppressed. These considerations motivate performing a comparison of the allowed 2HDM parameter space for both types of spectra, assessing the impact of sizeable mass splitting(s). In this respect, key probes of 2HDM scenarios are ATLAS/CMS measurements of Higgs signal strengths and searches for new scalar states at the LHC.

A. Higgs Signal Strengths in the 2HDM

The values for the Higgs signal strengths measured by the ATLAS and CMS experiments during the 7 and 8 TeV LHC runs set an important constraint on the 2HDM parameter space [9] (see also [10–18]). The model prediction for the signal strength in a final state xx is given by $\mu_{xx}^{2\text{HDM}} = \sum_i \epsilon_i \times \mu_{xx}^i$, with ϵ_i corresponding to the relative contribution to the signal from a particular Higgs production mode i , and μ_{xx}^i being the 2HDM signal strength for that production mode

$$\mu_{xx}^i = \frac{[\sigma_i(pp \rightarrow h) \times \text{BR}(h \rightarrow xx)]_{2\text{HDM}}}{[\sigma_i(pp \rightarrow h) \times \text{BR}(h \rightarrow xx)]_{\text{SM}}}, \quad (13)$$

to be compared with the values obtained by ATLAS and CMS analyses in the relevant detection channels, namely $h \rightarrow WW^*$ [34–38], $h \rightarrow ZZ^*$ [35, 39, 40], $h \rightarrow \gamma\gamma$ [41, 42], $h \rightarrow \bar{b}b$ [43, 44] and $h \rightarrow \tau\tau$ [45, 46]. In all but one of these channels the various μ_{xx}^i are directly obtained from the κ_x^h factors in (3) and (4), depending only on $c_{\beta-\alpha}$ and t_β . The sole exception is $\mu_{\gamma\gamma}^i$, since $\text{BR}(h \rightarrow \gamma\gamma)$ also involves the contribution to the $h \rightarrow \gamma\gamma$ decay amplitude from the charged scalar loop, Δ_γ^\pm , which introduces a dependence on μ^2 and other physical parameters via the trilinear $\lambda_{hH^+H^-}$. As a result, a comparison to the experimental data would strictly speaking require a generalized $\Delta\chi^2$ likelihood fit in a multidimensional parameter space subject to the theoretical constraints on μ^2 above discussed. However, since the charged scalar loop generically gives a very subdominant contribution, we adopt here a simplified approach of neglecting this term by setting $\lambda_{hH^+H^-} = 0$. The Higgs signals constraints can then be obtained by performing a $\Delta\chi^2$ likelihood fit to the 2HDM parameters $c_{\beta-\alpha}$ and t_β , for which we use the public codes LILITH [31] and HIGGSSIGNALS [32, 33]. The values of ϵ_i in (13) may be obtained from the experimental analyses and are provided in both these programs (*e.g.* for HIGGSSIGNALS they may be found in Appendix A of [33]).

The results are shown in Figure 1 for Type I (*Left*) and Type II (*Right*) 2HDM. The green areas correspond to the 95% C.L. allowed region from LILITH, while the hatched-purple ones are those from HIGGSSIGNALS. Both show good agreement with the ATLAS experimental fit [9], the fit from LILITH being slightly more constraining than both HIGGSSIGNALS and ATLAS. In Type I, a sizable departure from alignment is allowed as soon as $t_\beta \gtrsim 1$, and the limit on $c_{\beta-\alpha}$ becomes both independent of t_β and symmetric around $c_{\beta-\alpha} = 0$ for $t_\beta \gg 1$, which can be understood from (3). For Type II, there are two distinct allowed regions: (*i*) the region close to the alignment limit $c_{\beta-\alpha} \ll 1$ corresponding to a SM-like Higgs h , with a mild preference for $c_{\beta-\alpha} > 0$ and $t_\beta \sim 1$; (*ii*) the *wrong-sign* scenario $s_{\beta+\alpha} \sim 1$, for which $\kappa_d^h < 0$, and $0 < 1 + \kappa_d^h \ll 1$ (see *e.g.* [47] for a detailed discussion of this limit, possible only in Type II).

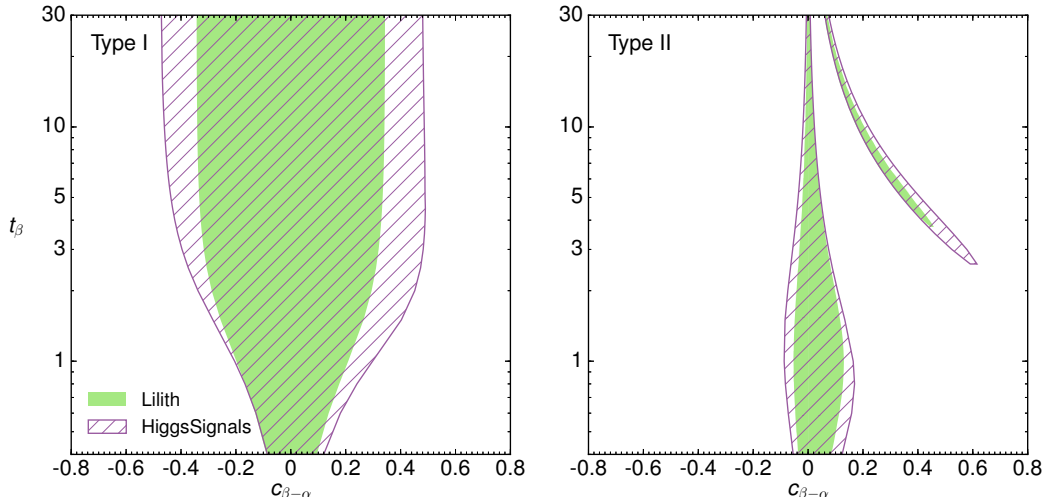


FIG. 1. 95% C.L. Likelihood fit to Higgs signal strengths in the $(c_{\beta-\alpha}, t_\beta)$ plane, for Type I (Left) and Type II (Right) 2HDM, using LILITH (solid-green region) and HIGGSSIGNALS (hatched-purple region). See text for details on the fit.

B. LHC Searches for A_0 into SM States

We discuss now the limits on the 2HDM parameter space from ATLAS and CMS searches of A_0 decaying via $A_0 \rightarrow Zh$ ($h \rightarrow \bar{b}b, h \rightarrow \tau\tau$) [48, 49], via $A_0 \rightarrow \gamma\gamma$ [50, 51] and $A_0 \rightarrow \tau\tau$ [52, 53]. For the $A_0 \rightarrow \tau\tau$ searches, the production of A_0 in association with a $\bar{b}b$ pair is taken into account by the ATLAS/CMS experimental analyses in addition to production through gluon fusion, the former being important for Type II at large values of t_β . Furthermore, we stress that while the search via $A_0 \rightarrow Zh$ vetoes any b-tagged jets beyond those from $h \rightarrow \bar{b}b$ (see *e.g.* [48]), the b-jets resulting from the $pp \rightarrow \bar{b}b A_0$ process generically have large rapidity values and consequently yield a very low b-tagging efficiency [54]. Thus we also consider $\bar{b}b$ -associated production of A_0 in the $A_0 \rightarrow Zh$ searches, and do not implement a b-tagging efficiency suppression in this case.

In order to derive the bounds on the 2HDM parameter space, we compute the A_0 production cross-section in gluon fusion and in association with $\bar{b}b$ at NNLO in QCD with SUSHI [55]) for Types I and II as a function of t_β and m_{A_0} , and then use 2HDMC [56] to compute the branching fractions for $A_0 \rightarrow \tau\tau$, $A_0 \rightarrow \gamma\gamma$, $A_0 \rightarrow Zh$ and $h \rightarrow \bar{b}b, \tau\tau$ as a function of t_β , $c_{\beta-\alpha}$, m_{A_0} and m_{H_0} . The 95% C.L. exclusion region in the $(c_{\beta-\alpha}, t_\beta)$ plane resulting from these searches is shown in Figure 2 for different values of m_{A_0} and $m_{A_0} - m_{H_0}$, and discussed below.

Let us consider first a high mass scenario for A_0 , above the $t\bar{t}$ threshold: The exclusion region for $m_{A_0} = 500$ GeV in Types I and II is shown respectively in Figure 2 (Top-Left) and (Top-Right). The only sensitive channel above the $t\bar{t}$ threshold is $A_0 \rightarrow Zh$, and for Type II also $A_0 \rightarrow \tau\tau$ in $\bar{b}b$ -associated production. Neverthe-

less, we see that for low/moderate t_β , these searches only constrain values of $|c_{\beta-\alpha}| \gtrsim 0.15$. The green region corresponds to the exclusion for $m_{H_0} = 500$ GeV, when A_0 can only decay into SM states. As m_{H_0} decreases and the decay $A_0 \rightarrow H_0 Z$ becomes kinematically allowed, the current limits from searches of SM decay channels weaken significantly, as the orange and purple regions in Figure 2 (Top) show respectively for $m_{H_0} = 300$ GeV and $m_{H_0} = 150$ GeV.

The impact of a sizable $m_{A_0} - m_{H_0}$ splitting is even more important for m_{A_0} below the $t\bar{t}$ threshold: The excluded region for $m_{A_0} = 300$ GeV is shown in Figure 2 (Medium) for Type I (Left) and Type II (Right), both in the degenerate scenario $m_{H_0} = 300$ GeV (green region) and for a hierarchical scenario with $m_{H_0} = 150$ GeV (purple region). In the former, the limits from $A_0 \rightarrow Zh$ searches are stringent, ruling out $|c_{\beta-\alpha}| \gtrsim 0.02$ for $t_\beta < 6$ in Type I. Even for $c_{\beta-\alpha} \rightarrow 0$, $A_0 \rightarrow \gamma\gamma$ and $A_0 \rightarrow \tau\tau$ searches constrain the region of $t_\beta \lesssim 2$ and $t_\beta \lesssim 3$ respectively for Types I and II. In contrast, for the hierarchical scenario the $A_0 \rightarrow \gamma\gamma$ and $A_0 \rightarrow \tau\tau$ searches only constrain values of $t_\beta \lesssim 0.5$, while the sensitivity of the $A_0 \rightarrow Zh$ searches also reduces drastically.

Finally, we also present the limits for a light A_0 , with $m_{A_0} = 150$ GeV in Figure 2 (Bottom). In this case we do not consider a hierarchical 2HDM scenario (with A_0 being the heavier state), as it would require $c_{\beta-\alpha} \rightarrow 0$ to avoid non-observation of H_0 at LEP (we will however briefly discuss this region of parameter space in Section III E). Both for Type I (Left) and Type II (Right), the $A_0 \rightarrow \tau\tau$ and $A_0 \rightarrow \gamma\gamma$ searches yield the constraint $t_\beta \gtrsim 1.5$, while for Type II the searches for $A_0 \rightarrow \tau\tau$ in $\bar{b}b$ -associated production also yield a limit $t_\beta < 10$.

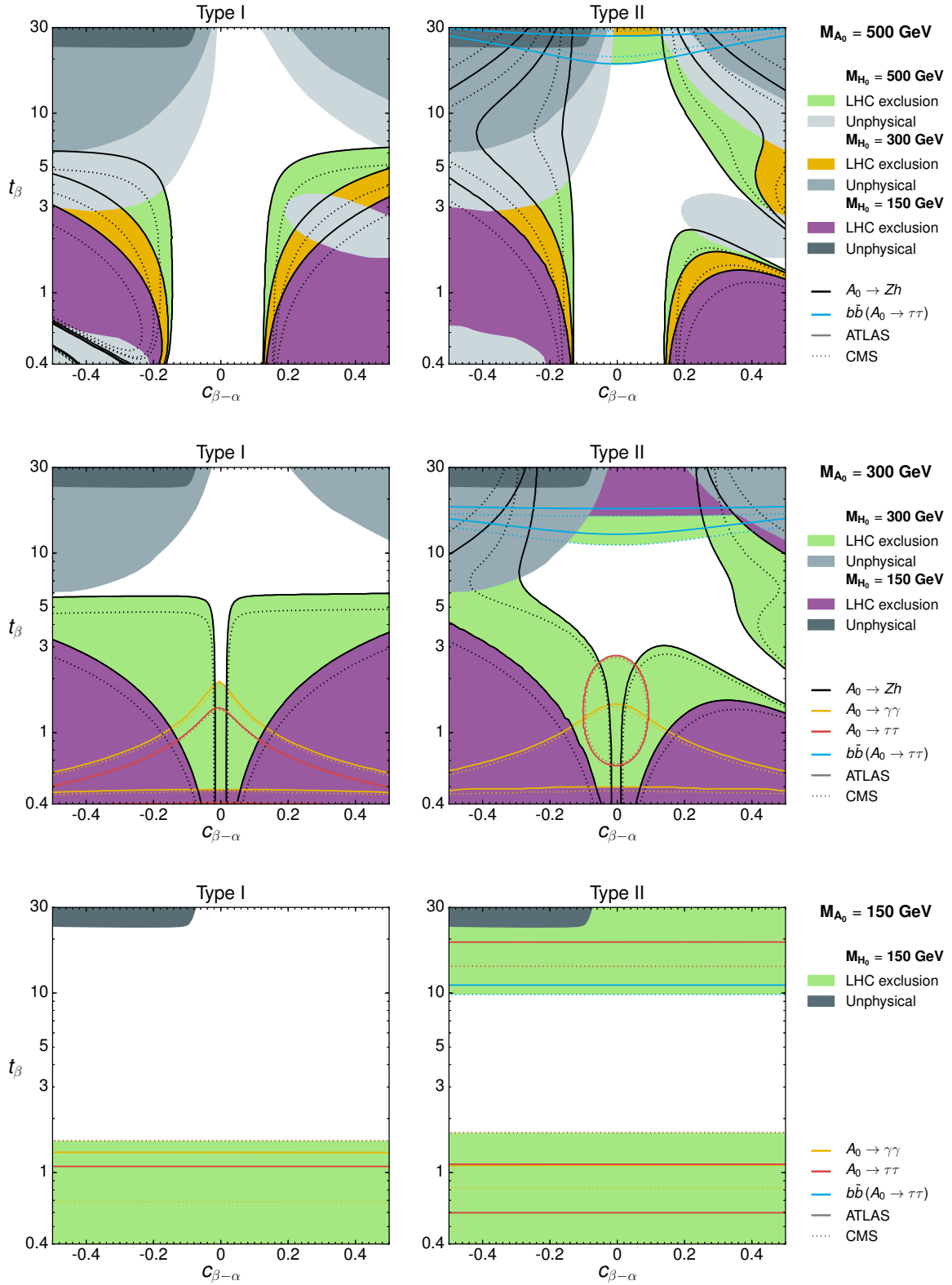


FIG. 2. Current 95% C.L. excluded region by ATLAS (solid lines) and CMS (dashed lines), respectively for $m_{A_0} = 500, 300, 150$ GeV (Top/Medium/Bottom) and for 2HDM Type I/II (Left/Right), coming from searches of $gg, b\bar{b} \rightarrow A_0 \rightarrow Zh$ ($h \rightarrow b\bar{b}$) (black lines), $gg \rightarrow A_0 \rightarrow \gamma\gamma$ (yellow lines), $gg \rightarrow A_0 \rightarrow \tau\tau$ (red lines) and $b\bar{b} \rightarrow A_0 \rightarrow \tau\tau$ (light-blue lines). In each case, the limits in the degenerate scenario $m_{H_0} = m_{A_0}$ are shown in green, while those for the hierarchical scenario(s) are shown in purple/orange. The various grey regions correspond to the theoretically excluded regions for the degenerate and hierarchical 2HDM scenarios (darker grey as m_{H_0} is lower).

The above discussion highlights the fact that, in the presence of a sizable mass splitting $m_{A_0} - m_{H_0}$, searches for A_0 decaying into SM final states have little sensitivity, and in particular do not yield further information on the allowed 2HDM parameter space to that obtained from Higgs coupling measurements, discussed in the previous Section. Let us however emphasize that the lighter state in the hierarchical 2HDM scenario, in this case H_0 , would decay solely into SM states. Thus, the constraints on the parameter space from searches of H_0 into SM final states would fully apply for a hierarchical scenario with $m_{A_0} - m_{H_0} > 0$. LHC searches for H_0 will be analyzed in Section III C.

Before moving on to the next Section, let us discuss the impact of theoretical constraints from unitarity, perturbativity and stability of the 2HDM scalar potential on Figure 2, where the theoretically excluded regions are shown in grey. Focusing on the case $m_{H^\pm} = m_{A_0}$, and defining $m_{A_0}^2 - m_{H_0}^2 \equiv \Delta^2 \geq 0$, Figure 2 shows that the exclusion becomes more important as m_{H_0} increases, particularly for $t_\beta \gg 1$. The departure from alignment also has a strong impact on the theoretically viable parameter space, specially for $c_{\beta-\alpha} < 0$. These features may be understood from the interplay of $\lambda_1 > 0$ and various unitarity limits. Writing λ_1 as

$$\lambda_1 v^2 = m_h^2 - t_\beta(1 + t_\beta^2) \Omega^2 - (m_{H_0}^2 - m_h^2) [c_{\beta-\alpha}^2(t_\beta^2 - 1) - 2t_\beta s_{\beta-\alpha} c_{\beta-\alpha}] \quad (14)$$

with $\Omega^2 \equiv \mu^2 - m_{H_0}^2 s_\beta c_\beta$, we see that for $m_{H_0}^2 \gg m_h^2$ (neglecting m_h^2 in (14)) and $t_\beta > 1$, $\Omega^2 < 0$ is required to satisfy $\lambda_1 > 0$ for either $c_{\beta-\alpha} < 0$ or $c_{\beta-\alpha} t_\beta \gg 1$. This in turn impacts the unitarity requirements, *e.g.*

$$|\lambda_3 + \lambda_4| \sim \left| \frac{\Delta^2}{v^2} + \frac{m_{H_0}^2 c_{\beta-\alpha}}{v^2} [s_{\beta-\alpha}(t_\beta - t_\beta^{-1}) - 2c_{\beta-\alpha}] \right| < 8\pi$$

$$|\lambda_3 + 2\lambda_4 + 3\lambda_5| \sim \left| -\frac{3\Delta^2}{v^2} + \frac{4}{s_\beta c_\beta} \frac{\Omega^2}{v^2} + \frac{m_{H_0}^2}{v^2} c_{\beta-\alpha} [s_{\beta-\alpha}(t_\beta - t_\beta^{-1}) - 2c_{\beta-\alpha}] \right| < 8\pi \quad (15)$$

which are then violated for $t_\beta \gg 1$ and/or $m_{H_0}^2 \gg v^2$, as no cancellation among terms is possible in both $|\lambda_3 + \lambda_4|$ and $|\lambda_3 + 2\lambda_4 + 3\lambda_5|$ (since $\Delta^2 \geq 0$, $\Omega^2 < 0$).

We note that the above requirement $\Omega^2 < 0$ to satisfy $\lambda_1 > 0$ may be avoided for $c_{\beta-\alpha}(t_\beta^2 - 1) - 2t_\beta s_{\beta-\alpha} \sim 0$, for which the last term in (14) vanishes. This cancellation, which happens for $c_{\beta-\alpha} = 2t_\beta/(1 + t_\beta^2)$, is observed for $m_{H_0}^2 = 500$ GeV and $c_{\beta-\alpha} > 0$ in Figure 2 (Top). We also note that in exact alignment $c_{\beta-\alpha} = 0$, $\Omega^2 = 0$ automatically yields $\lambda_1 > 0$ (and all other boundedness-from-below requirements are also trivially satisfied for $\Delta^2 \geq 0$). The unitarity constraints are then only violated for $\Delta^2 \gg v^2$, and thus $c_{\beta-\alpha} = 0$ is always allowed in Figure 2.

C. LHC Searches for H_0 into SM States

We turn on now to analyze the constraints from LHC searches for H_0 . The relevant searches to be considered are $H_0 \rightarrow ZZ \rightarrow \ell\ell\ell\ell$ [57] (and in the low mass region also $H_0 \rightarrow WW$ [58]), $H_0 \rightarrow hh \rightarrow \bar{b}b\gamma\gamma$ [59] by ATLAS and $H_0 \rightarrow WW, ZZ$ [60] (both low and high mass region), $H_0 \rightarrow hh \rightarrow \bar{b}b\gamma\gamma$ [61] and $H_0 \rightarrow hh \rightarrow \bar{b}bbb$ [62] by CMS. In all these searches, $\bar{b}b$ -associated production of H_0 is implicitly included² together with gluon fusion. In addition, the ATLAS/CMS searches via $A_0/H_0 \rightarrow \gamma\gamma$ [50, 51] and via $A_0/H_0 \rightarrow \tau\tau$ [52, 53] discussed in the previous Section also apply in this case.

As in the previous section, we use SUSHi to compute the gluon fusion and $\bar{b}b$ -associated H_0 production cross-sections at NNLO in QCD for Types I and II as a function of $c_{\beta-\alpha}$, t_β and m_{H_0} , and then use 2HDMC to compute the branching fractions for $H_0 \rightarrow \tau\tau$, $H_0 \rightarrow \gamma\gamma$, $H_0 \rightarrow ZZ$, $H_0 \rightarrow hh$ and $h \rightarrow \bar{b}b, \gamma\gamma$ as a function of $c_{\beta-\alpha}$, t_β , m_{H_0} , m_{A_0} and μ^2 . We stress that, contrary to the A_0 case, the value of μ^2 has a significant impact on the H_0 branching fractions via the modification of the trilinear coupling $\lambda_{H_0 hh}$, which changes the $H_0 \rightarrow hh$ partial width (recall the discussion at the end of Section II). In order to account for the dependence of μ^2 on the 95% C.L. limits, we compute the theoretically viable μ^2 range as a function of $c_{\beta-\alpha}$, t_β , m_{H_0} and m_{A_0} , and derive the bounds on the values of μ^2 that respectively minimize (μ_{\min}^2) and maximize (μ_{\max}^2) the $H_0 \rightarrow hh$ branching fraction within the allowed μ^2 range.

We begin now by discussing the scenario with a light H_0 , and consider the 95% C.L. exclusion region for $m_{H_0} = 150$ GeV in the degenerate scenario, as shown in Figure 3. Due to the absence of the $H_0 \rightarrow hh$ decay in this case, the $H_0 \rightarrow ZZ^*$ and $H_0 \rightarrow \tau\tau$ branching fractions are not sensitive to the value of μ^2 , and only $H_0 \rightarrow \gamma\gamma$ is mildly dependent via the H^\pm loop contribution. Nevertheless, Figure 3 shows that the important limits in the $c_{\beta-\alpha}$, t_β plane are given by $H_0 \rightarrow ZZ^*$ and $H_0 \rightarrow \tau\tau$ searches, with $H_0 \rightarrow \gamma\gamma$ less sensitive. As has been emphasized in Section III B, the present limits are complementary to those from A_0 searches in the hierarchical 2HDM, *e.g.* for the $(m_{A_0}, m_{H_0}) = (300, 150)$ GeV and $(500, 150)$ GeV benchmarks considered in Figure 2.

In Figure 4 we show the limits from H_0 searches for $m_{H_0} = 300$ GeV, for Type I/II (Left/Right). Here, the presence of the decay $H_0 \rightarrow hh$ requires us to take into account the μ^2 dependence in the limit extraction, and we show the limits for $\mu^2 = \mu_{\min}^2$ (Top) and $\mu^2 = \mu_{\max}^2$ (Bottom). In the former case the strongest limits come from $H_0 \rightarrow ZZ$ searches, with $H_0 \rightarrow hh$ playing no relevant role because of its suppressed branching fraction.

² For $H_0 \rightarrow WW, ZZ$ searches, $\bar{b}b$ -associated production generally fails the Vector Boson Fusion and V -associated production analysis tags, and so is included in the gluon fusion category. For $H_0 \rightarrow hh$ searches, the analysis is inclusive *w.r.t.* H_0 production.

Moreover, in this case the presence of a sizable $m_{H_0} - m_{A_0}$ splitting does lead to a significant reduction of the limits on the 2HDM parameter space from these searches. In contrast, for $\mu^2 = \mu_{\max}^2$ the $H_0 \rightarrow hh$ searches provide the dominant constraint for low and moderate t_β , and these limits do not change significantly in a hierarchical 2HDM scenario, as the branching fraction of $H_0 \rightarrow hh$ is still the dominant one in this case. A similar situation occurs for $m_{H_0} = 500$ GeV, as shown in Figure 5. Again, for $\mu^2 = \mu_{\min}^2$ (Top) $H_0 \rightarrow ZZ$ searches provide the only meaningful constraint, which gets significantly weakened in the hierarchical scenario $m_{H_0} - m_{A_0} \gg m_Z$. For $\mu^2 = \mu_{\max}^2$ the LHC searches for $H_0 \rightarrow hh$ in $b\bar{b}b\bar{b}$ and $b\bar{b}\gamma\gamma$ are the most constraining, being particularly

sensitive around $t_\beta \sim 1$, and the limits only get mildly weakened in the hierarchical 2HDM scenario. In addition, for $m_{H_0} = 500$ GeV there is no appreciable difference between Types I and II for low and moderate t_β , with $b\bar{b}$ -associated production of H_0 in $H_0 \rightarrow \tau\tau$ searches constraining the $t_\beta \gg 1$ region in Type II.

Contrary to Figure 2, Figures 4-5 do not show the would-be limits on the $(c_{\beta-\alpha}, t_\beta)$ plane from searches of H_0 in regions which are not viable theoretically: These limits depend crucially on the value of μ^2 (in contrast with the situation for A_0 searches discussed in Section III B), and the theoretical bounds correspond precisely to the absence of an allowed μ^2 range.

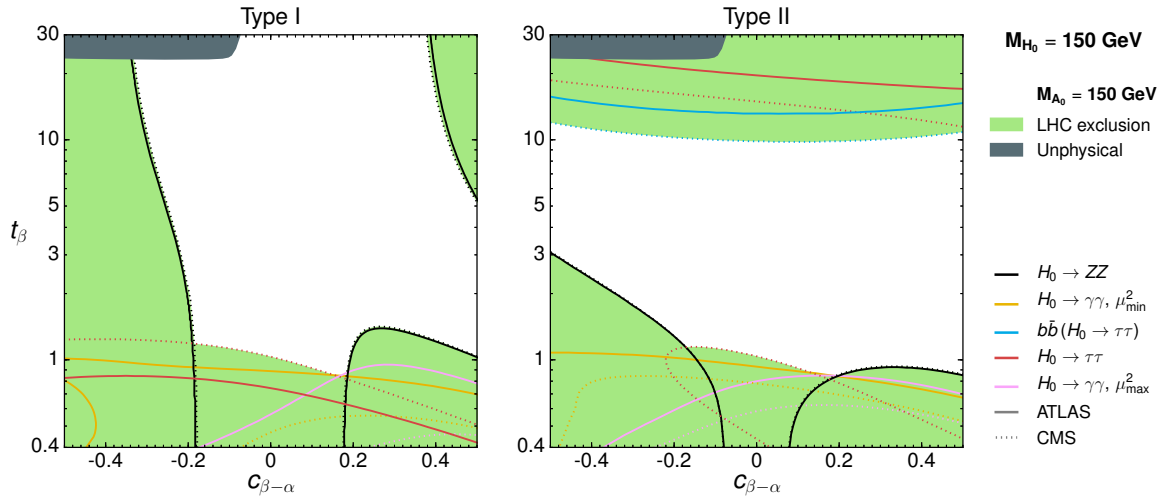


FIG. 3. Current 95% C.L. excluded region (in green) by ATLAS (solid lines) and CMS (dashed lines), respectively for $m_{H_0} = 150$ GeV and 2HDM Type I/II (Left/Right), coming from searches of $gg, b\bar{b} \rightarrow H_0 \rightarrow WW, ZZ$ (black lines), $gg \rightarrow A_0 \rightarrow \tau\tau$ (red lines), $b\bar{b} \rightarrow A_0 \rightarrow \tau\tau$ (light-blue lines) and $gg \rightarrow A_0 \rightarrow \gamma\gamma$ respectively for $\mu^2 = \mu_{\min}^2 / \mu^2 = \mu_{\max}^2$ (yellow/pink lines). The grey region is theoretically excluded.

Figures 4-5 highlight that, for $\Delta^2 < 0$ (and $m_{H^\pm}^2 = m_{H_0}^2$), the theoretical bounds from stability, unitarity and perturbativity are significantly more important than for the previously discussed $\Delta^2 > 0$ case, and in particular constrain the alignment limit $c_{\beta-\alpha} = 0$. The stability conditions for $c_{\beta-\alpha} = 0$ read

$$\begin{aligned} \lambda_1 &= \frac{m_h^2}{v^2} - t_\beta(1+t_\beta^2) \frac{\Omega^2}{v^2} > 0 \\ \lambda_2 &= \frac{m_h^2}{v^2} - \frac{(1+t_\beta^{-2})}{t_\beta} \frac{\Omega^2}{v^2} > 0 \\ \lambda_3 &= \frac{m_h^2}{v^2} - \frac{1}{s_\beta c_\beta} \frac{\Omega^2}{v^2} > -\sqrt{\lambda_1 \lambda_2} \\ \lambda_3 + \lambda_4 - |\lambda_5| &= \frac{m_h^2}{v^2} + \frac{\Delta^2}{v^2} - \left| \frac{1}{s_\beta c_\beta} \frac{\Omega^2}{v^2} - \frac{\Delta^2}{v^2} \right| > -\sqrt{\lambda_1 \lambda_2} \end{aligned} \quad (16)$$

The first three inequalities in (16) are trivially satisfied for $\Omega^2 \leq 0$. For $|\Delta^2| \gg v^2$ the last one however requires $\Omega^2 \sim s_\beta c_\beta \Delta^2$, and this affects the unitarity bounds which depend on $\lambda_1 + \lambda_2$, *e.g.*

$$\begin{aligned} \left| \lambda_1 + \lambda_2 + \sqrt{(\lambda_1 - \lambda_2)^2 + 4\lambda_4^2} \right| &\sim 2 \frac{|\Delta^2| t_\beta^2}{v^2} \quad (t_\beta \gg 1) \\ &\sim 2 \frac{|\Delta^2|}{v^2 t_\beta^2} \quad (t_\beta \ll 1) \end{aligned} \quad (17)$$

such that only values $t_\beta \sim 1$ are allowed if $|\Delta^2| \gg v^2$.

D. Comments on H^\pm Searches at LHC

Before we comment on the limits from direct searches of H^\pm , let us emphasize that there are two other important sources of constraints on the mass of H^\pm in this case:

(i) Flavour Physics yields important bounds on m_{H^\pm} , the most stringent one coming from the H^\pm contribution to the flavour violating decay $b \rightarrow s\gamma$. For Type II 2HDM, this leads to a lower bound $m_{H^\pm} > 480$ GeV at 95% C.L. [63], while for Type I the bound is milder and depends on t_β [64]. (ii) EWPO strongly prefer $m_{H^\pm} \sim m_{A_0}$ or $m_{H^\pm} \sim m_{H_0}$ (this last condition is mildly modified away from the alignment limit $c_{\beta-\alpha} = 0$), as a splitting between the charged and neutral components of the doublet breaks custodial symmetry. While some degree of splitting is allowed by EWPO, it cannot be sizable (see *e.g.* the analysis of [19]). In the present work we have chosen for simplicity to make H^\pm degenerate with the heavier of the two neutral scalars H_0, A_0 , as neglecting small mass splittings between the charged and

neutral scalars does not have an appreciable impact on the theoretical constraints on the model, nor on the phenomenological analysis, and satisfies EWPO. Regarding the bounds from Flavour Physics, while particularly for Type II they motivate our choice of pairing H^\pm with the heavier state among H_0, A_0 , we do not consider them as limits *stricto sensu*, meaning that for Type II we still discuss scenarios in which both m_{A_0} and m_{H_0} are below 480 GeV. We also stress that, since for Type I the $b \rightarrow s\gamma$ bound is not as severe, it could be possible for H^\pm to pair with the lighter state among H_0, A_0 . For a hierarchical 2HDM scenario, this would also open either the decay $A_0 \rightarrow W^\pm H^\pm$ or $H_0 \rightarrow W^\pm H^\pm$, and would make the LHC limits from searches of A_0, H_0 into SM states even weaker, opening at the same time further opportunities for direct searches of these new states (see *e.g.* [29, 30]).

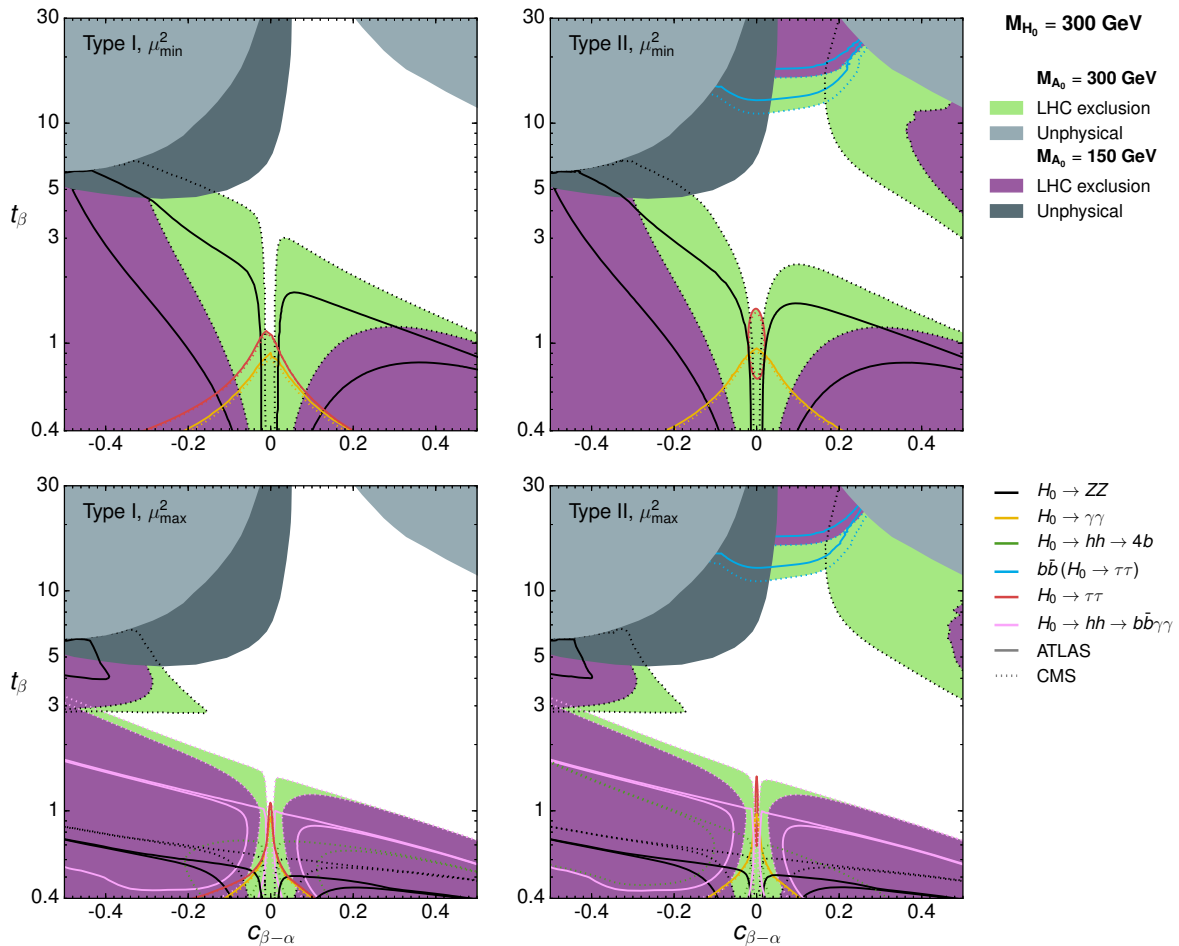


FIG. 4. Current 95% C.L. excluded region by ATLAS (solid lines) and CMS (dashed lines) for $m_{H_0} = 300$ GeV and respectively for 2HDM Type I/II (Left/Right) in the case $\mu^2 = \mu_{\min}^2/\mu^2 = \mu_{\max}^2$ (Top/Bottom). The limits come from searches of $gg, b\bar{b} \rightarrow H_0 \rightarrow WW, ZZ$ (black lines), $gg \rightarrow A_0 \rightarrow \tau\tau$ (red lines), $b\bar{b} \rightarrow A_0 \rightarrow \tau\tau$ (light-blue lines), $gg \rightarrow A_0 \rightarrow \gamma\gamma$ (yellow lines), $gg, b\bar{b} \rightarrow H_0 \rightarrow hh \rightarrow b\bar{b}b\bar{b}$ (dark-green lines) and $gg, b\bar{b} \rightarrow H_0 \rightarrow hh \rightarrow b\bar{b}\gamma\gamma$ (pink lines). The two scenarios considered are $m_{H_0} = m_{A_0}$ (Degenerate: green exclusion region) and $m_{H_0} - m_{A_0} = 150$ GeV (Hierarchical: purple exclusion region). The light/dark grey areas correspond to the theoretically excluded regions for the degenerate/hierarchical 2HDM scenarios.

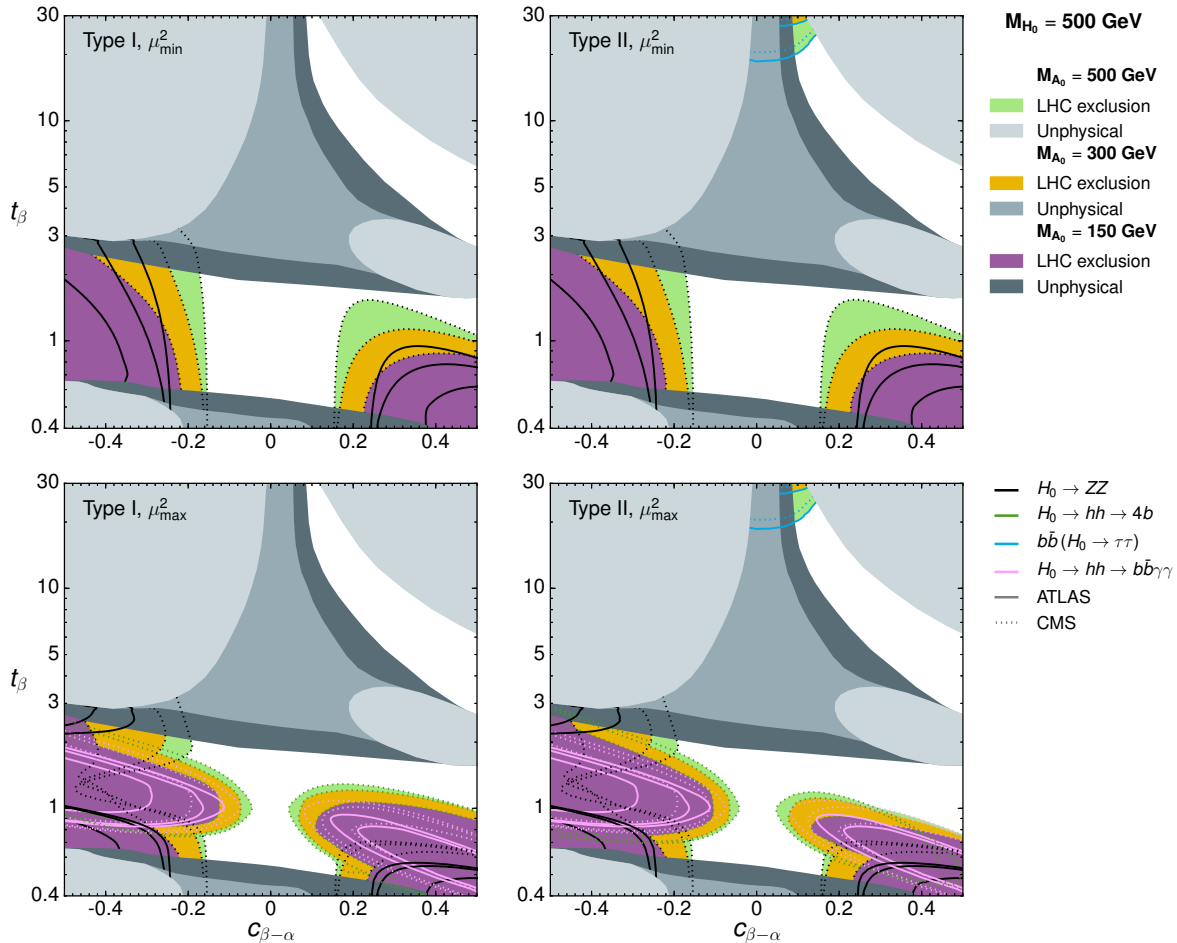


FIG. 5. Current 95% C.L. excluded region by ATLAS (solid lines) and CMS (dashed lines) for $m_{H_0} = 500$ GeV and respectively for 2HDM Type I/II (Left/Right) in the case $\mu^2 = \mu_{\min}^2/\mu^2 = \mu_{\max}^2$ (Top/Bottom). The limits come from searches of $gg, b\bar{b} \rightarrow H_0 \rightarrow WW, ZZ$ (black lines), $b\bar{b} \rightarrow A_0 \rightarrow \tau\tau$ (light-blue lines), $gg, b\bar{b} \rightarrow H_0 \rightarrow hh \rightarrow b\bar{b}b\bar{b}$ (dark-green lines) and $gg, b\bar{b} \rightarrow H_0 \rightarrow hh \rightarrow b\bar{b}\gamma\gamma$ (pink lines). The two scenarios considered are $m_{H_0} = m_{A_0}$ (Degenerate: green exclusion region) and $m_{H_0} - m_{A_0} = 150$ GeV (Hierarchical: purple exclusion region). The light/dark grey areas correspond to the theoretically excluded regions for the degenerate/hierarchical 2HDM scenarios.

We now briefly discuss the current bounds from searches of H^\pm by ATLAS and CMS. For a light H^\pm , $m_{H^\pm} < m_t = 173$ GeV, ATLAS searches for $t \rightarrow H^\pm b$ in top quark pair production with the full dataset of Run 1 [65, 66] set a 95% C.L. bound on the branching fraction $\text{BR}(t \rightarrow H^\pm b) \times \text{BR}(H^\pm \rightarrow \nu\tau) < [0.0023, 0.013]$ in the mass range $m_{H^\pm} \in [80 \text{ GeV}, 160 \text{ GeV}]$. For $m_{H^\pm} > m_t$, ATLAS searches for H^\pm produced in association with a top quark [66] yield the bound $\sigma(pp \rightarrow tH^\pm + X) \times \text{BR}(H^\pm \rightarrow \nu\tau) < [0.76 \text{ pb}, 4.5 \text{ fb}]$ in the range $m_{H^\pm} \in [180 \text{ GeV}, 1000 \text{ GeV}]$. We however note that these bounds do not result generically in meaningful constraints, since $\text{BR}(H^\pm \rightarrow \nu\tau) \ll 1$ when the decay $H^\pm \rightarrow tb$ is open. Moreover, in the hierarchical scenario $\text{BR}(H^\pm \rightarrow \nu\tau)$ may be further suppressed by the presence of either $H^\pm \rightarrow W^\pm A_0$ or $H^\pm \rightarrow W^\pm H_0$ decays.

E. Filling the Gaps: $A_0 \rightarrow ZH_0/H_0 \rightarrow ZA_0$ Searches

Our previous analysis highlights that, while direct searches for heavy neutral Higgs bosons at the LHC may provide a wide coverage across the 2HDM parameter space, and complementary to measurements of signal strengths, bounds from searches assuming direct decays of the neutral scalars into SM particles become much weaker in a hierarchical 2HDM scenario, and new searches are needed to fill in the gaps. It is also clear that the new searches capable of probing a hierarchical 2HDM are precisely those which exploit the sizable mass splittings among the neutral scalars, namely³ $A_0 \rightarrow ZH_0$

³ Other decay modes could also be promising, like $A_0/H_0 \rightarrow W^\pm H^\pm$ or $H^\pm \rightarrow W^\pm A_0/H_0$, depending on m_{H^\pm} [29, 30]

or $H_0 \rightarrow ZA_0$. In the former case, the relevant final state to search for would depend on the dominant decay mode of H_0 [8]. For $c_{\beta-\alpha} \sim 0$, $H_0 \rightarrow b\bar{b}$ (eventually, $H_0 \rightarrow t\bar{t}$ if $m_{H_0} > 340$ GeV) would dominate, yielding $A_0 \rightarrow ZH_0 \rightarrow \ell\ell b\bar{b}$ as most sensitive final state. For a sizable departure from alignment, the dominant decay mode would be $H_0 \rightarrow W^+W^-$, yielding $A_0 \rightarrow ZH_0 \rightarrow \ell\ell W^+W^-$ ($W^+W^- \rightarrow \ell\nu \ell\nu$) as the most sensitive final state⁴.

For $H_0 \rightarrow ZA_0$, the most sensitive final state is generically $\ell\ell b\bar{b}$. In [20], the CMS Collaboration has performed

the first analysis of such signatures, with an integrated luminosity of $\mathcal{L} = 19.8 \text{ fb}^{-1}$ at 8 TeV, in the $\ell\ell b\bar{b}$ final state relevant for both $A_0 \rightarrow ZH_0$ and $H_0 \rightarrow ZA_0$. We discuss here the limits on the 2HDM parameter space that may be derived from that search. We stress that from the point of view of the CMS analysis, the limits on the production cross sections for $A_0 \rightarrow ZH_0$ and $H_0 \rightarrow ZA_0$ are identical for the same kinematical mass point. However, the translation between these limits and the constraints on the 2HDM parameter space is quite different in the two cases.

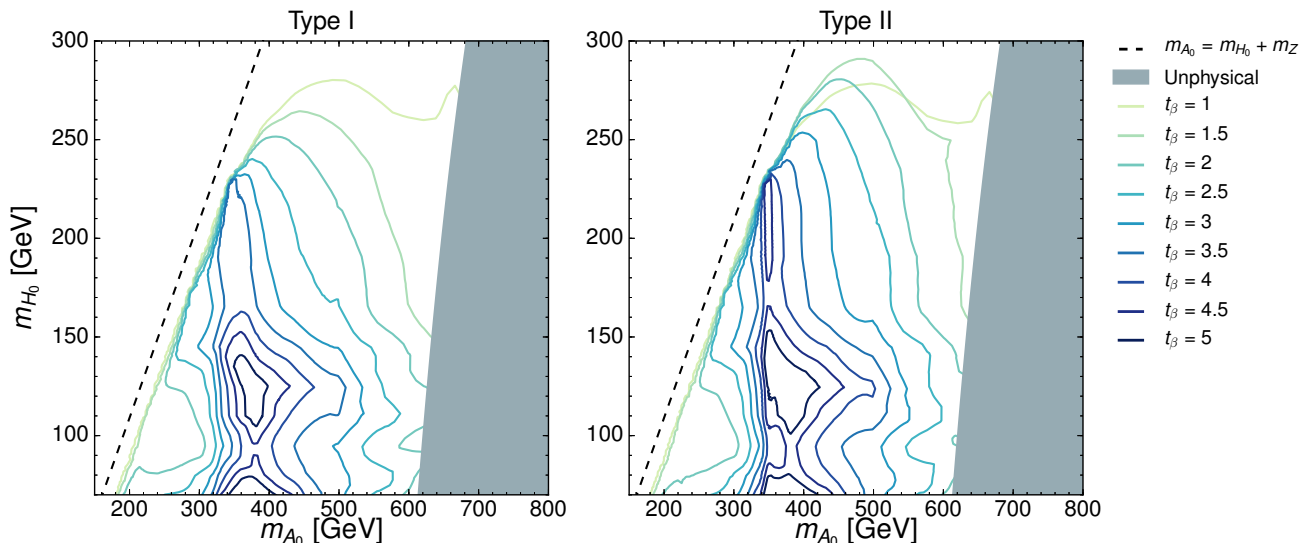


FIG. 6. Bounds on t_β in the (m_{A_0}, m_{H_0}) plane for $c_{\beta-\alpha} = 0$, from the search for $A_0 \rightarrow ZH_0 \rightarrow \ell\ell b\bar{b}$ performed in [20], For 2HDM of Type I (Left) and Type II (Right). The grey regions are theoretically excluded.

Concentrating first on $A_0 \rightarrow ZH_0$, we show in Figure 6 the bounds on t_β in the (m_{A_0}, m_{H_0}) plane for Type I (Left) and Type II (Right), assuming $c_{\beta-\alpha} = 0$. The search constrains up to $t_\beta \sim 5$ around $m_{A_0} = 380$ GeV, and additionally yields the limit $t_\beta \gtrsim 2$ for $m_{H_0} < 80$ GeV and $m_{A_0} < 600$ GeV. However, we expect a weakening of these limits once there is departure from the alignment limit, and we emphasize that searches for the $H_0 \rightarrow W^+W^-$ decay mode (and ZZ) are very much needed in this region (note that for $t_\beta^{-1}s_{\beta-\alpha} - c_{\beta-\alpha} \sim 0$, direct searches for $H_0 \rightarrow W^+W^-$ assuming gluon fusion production will not be sensitive to H_0).

In order to illustrate the complementarity between the above limits from $A_0 \rightarrow ZH_0$ searches and those from the most sensitive ATLAS/CMS searches for A_0, H_0 de-

caying directly into SM states analyzed in Sections III B and III C, as well as their interplay with measurements of Higgs signal strengths from Section III A (we take here the limits obtained with HIGSSIGNALS), we present a summary of the various bounds on the $(c_{\beta-\alpha}, t_\beta)$ plane in Figures 7 and 8 for Type I/II (Left/Right): Figure 7 (Top) shows the combined limits for $m_{A_0} = m_{H_0} = 150$ GeV (only the degenerate scenario is considered in this case). Focusing then on $m_{A_0} = 300$ GeV, Figure 7 (Bottom) highlights the fact that close to $c_{\beta-\alpha} = 0$ the CMS search for $A_0 \rightarrow ZH_0$ ($H_0 \rightarrow b\bar{b}$) in the hierarchical 2HDM scenario yields a superior sensitivity to the one obtained in the degenerate 2HDM scenario via the union of limits from A_0 and H_0 searches. It is also interesting to note that while in the degenerate scenario the combination of A_0 and H_0 searches exclude the Type II *wrong-sign* region allowed by Higgs signal strength measurements, in the hierarchical scenario the *wrong-sign* region is allowed by direct searches.

⁴ Other competitive final states are $H_0 \rightarrow W^+W^-$ ($W^+W^- \rightarrow \ell\nu jj$) and $H_0 \rightarrow ZZ$ yielding $A_0 \rightarrow ZH_0 \rightarrow \ell\ell' \ell' jj$ [28].

We note that for $m_{A_0} = 150$ GeV and $m_{A_0} = 300$ GeV the choice between $\mu^2 = \mu_{\min}^2$ and $\mu^2 = \mu_{\max}^2$ does not impact the limits shown in Figure 7 since the di-Higgs searches are not the most constraining in this plane. For $m_{A_0} = 500$ GeV the situation is different, as shown in Figure 8. Here, the degenerate case is the least constrained, cutting into the edges of the Type I light Higgs limits and not significantly affecting the Type II exclusions near alignment. In the μ_{\max} scenario, the di-Higgs

searches improve the limits towards alignment around $t_\beta \sim 1$. As one decreases the H_0 mass the picture changes considerably, with the direct H_0 searches proving particularly effective for $m_{H_0} = 300$ GeV, even near alignment. For $m_{H_0} = 150$ GeV, the $A_0 \rightarrow Z H_0$ becomes sensitive and provides excellent coverage up to $t_\beta \sim 3$, generally improving on the direct searches. We note, again, that the *wrong-sign* scenario in Type II is excluded in the degenerate and $m_{H_0} = 300$ GeV cases, while it is mostly allowed in the lightest H_0 case.

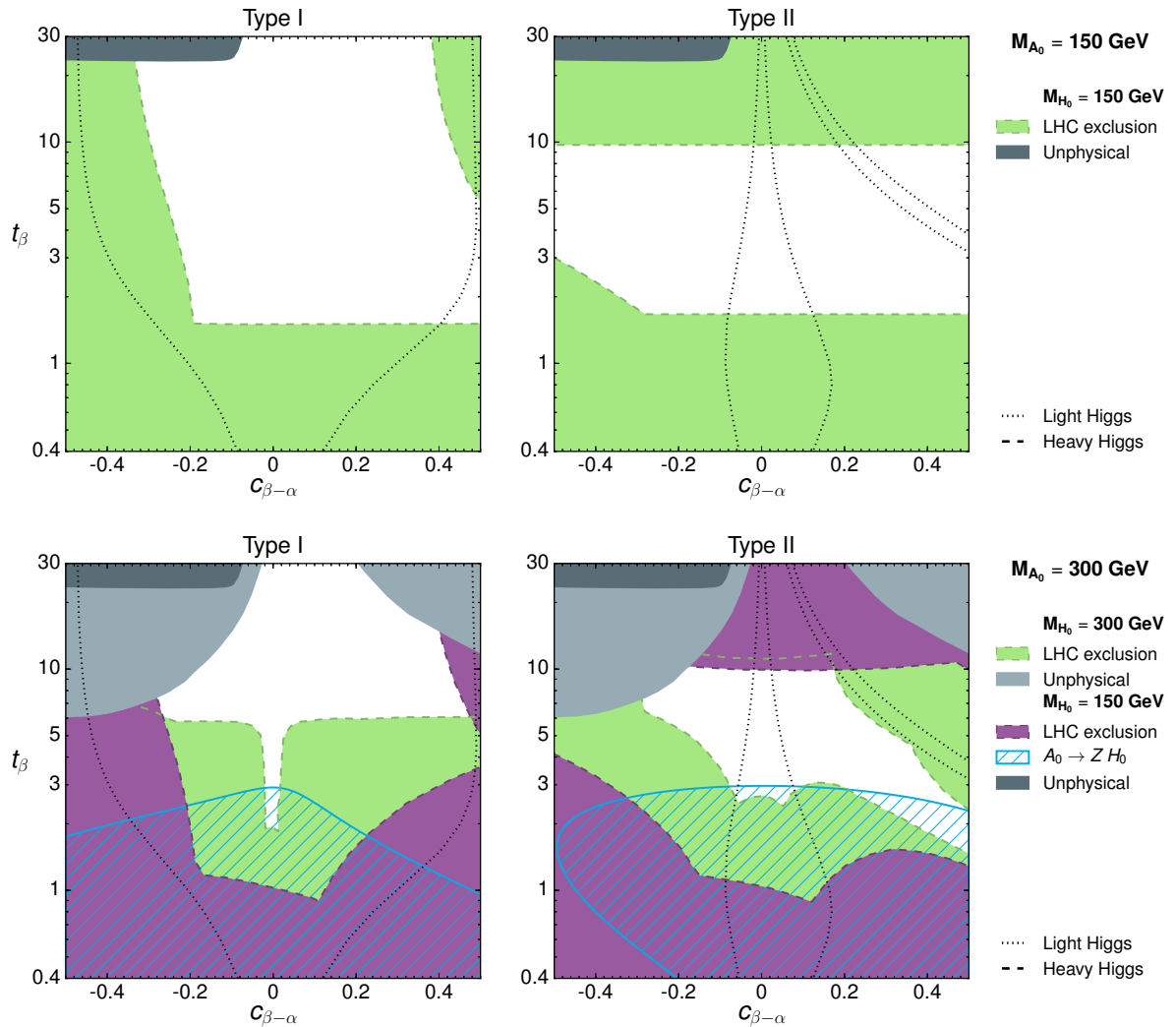


FIG. 7. Limits in the $(c_{\beta-\alpha}, t_\beta)$ plane for $m_{A_0} = 150/300$ GeV (Top/Bottom) and Type I/II (Left/Right), from measurements of Higgs signal strengths obtained with HIGGSIGNALS (dotted black lines; see Section III A) and from the most sensitive ATLAS/CMS searches for A_0 and H_0 decaying directly into SM states: green region corresponds to the exclusion in the degenerate scenario $m_{H_0} = m_{A_0}$; purple regions correspond to the exclusion in the hierarchical scenario (see Sections III B, III C). The dashed blue region corresponds to the exclusion from the CMS $A_0 \rightarrow Z H_0 \rightarrow \ell\ell b\bar{b}$ search [20] in the hierarchical scenario. The grey regions are theoretically excluded.

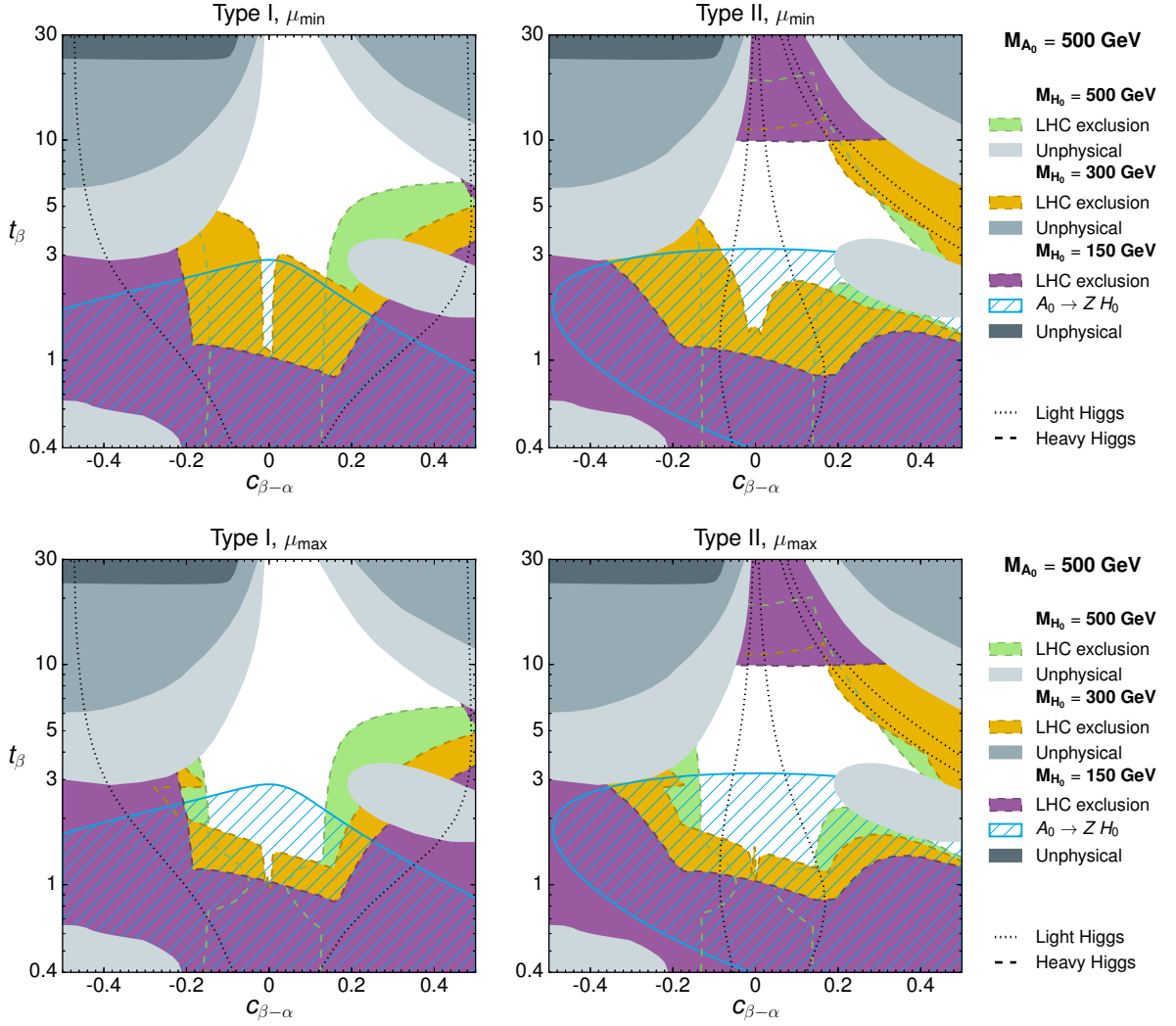


FIG. 8. Limits in the $(c_{\beta-\alpha}, t_\beta)$ plane for $m_{A_0} = 500$ GeV with $\mu^2 = \mu_{\min}^2/\mu^2 = \mu_{\max}^2$ (Top/Bottom) and Type I/II (Left/Right), from measurements of Higgs signal strengths obtained with HIGGSIGNALS (dotted black lines; see Section III A) and from the most sensitive ATLAS/CMS searches for A_0 and H_0 decaying directly into SM states: green region corresponds to the exclusion in the degenerate scenario $m_{H_0} = m_{A_0}$; purple/orange regions correspond to the exclusion in the hierarchical scenario(s) (see Sections III B, III C). The dashed blue region corresponds to the exclusion from the CMS $A_0 \rightarrow ZH_0 \rightarrow \ell\ell b\bar{b}$ search [20] in the hierarchical scenario $m_{H_0} = 150$ GeV. The grey regions are theoretically excluded.

Turning to $H_0 \rightarrow ZA_0$, we show the limits on t_β in the (m_{A_0}, m_{H_0}) plane in Figure 9, for Type I (Left) and Type II (Right) in the alignment limit. A few comments are in order: First, the limits are expected to be weaker than for $A_0 \rightarrow ZH_0$, as the production cross section for A_0 is larger than that for H_0 for the same mass. More importantly, when $m_{H_0} > 2m_{A_0}$, the decay $H_0 \rightarrow A_0A_0$ becomes kinematically possible, which weakens the bounds from $H_0 \rightarrow ZA_0$ and also makes them dependent on μ^2 , since $\text{BR}(H_0 \rightarrow A_0A_0)$ does depend on this parameter. Figure 9 (Top) shows the limits for $\mu^2 = \mu_{\min}^2$, while Figure 9 (Bottom) shows the limits for $\mu^2 = \mu_{\max}^2$ which are identical for $m_{H_0} < 2m_{A_0}$ but much weaker for $m_{H_0} > 2m_{A_0}$ as expected. Note

also that for $t_\beta = 1$ the limits are identical in both mass regions, since $\lambda_{H_0A_0A_0} = 0$ and the μ^2 dependence therefore disappears. In the region $m_{H_0} > 2m_{A_0}$, the width of H_0 very quickly reaches $\Gamma_{H_0}/m_{H_0} > 0.15$, for which the bounds from the analysis [20] are no longer robust (these regions are marked as shaded in Figure 9). This is in contrast with $A_0 \rightarrow ZH_0$ bounds, for which $\Gamma_{A_0}/m_{A_0} < 0.15$ throughout the whole allowed parameter space. From the comparison of Figures 6 and 9 it is also apparent that for a sizable splitting $m_{H_0} - m_{A_0} > 0$, the 2HDM parameter space is much more theoretically constrained than for a splitting $m_{A_0} - m_{H_0} > 0$ of same magnitude, and the constraints become more stringent as t_β increases (recall the discussion in Section III C), such that for $t_\beta > 2$ $m_{H_0} \lesssim 500$ GeV is required, as shown in Figure 9.

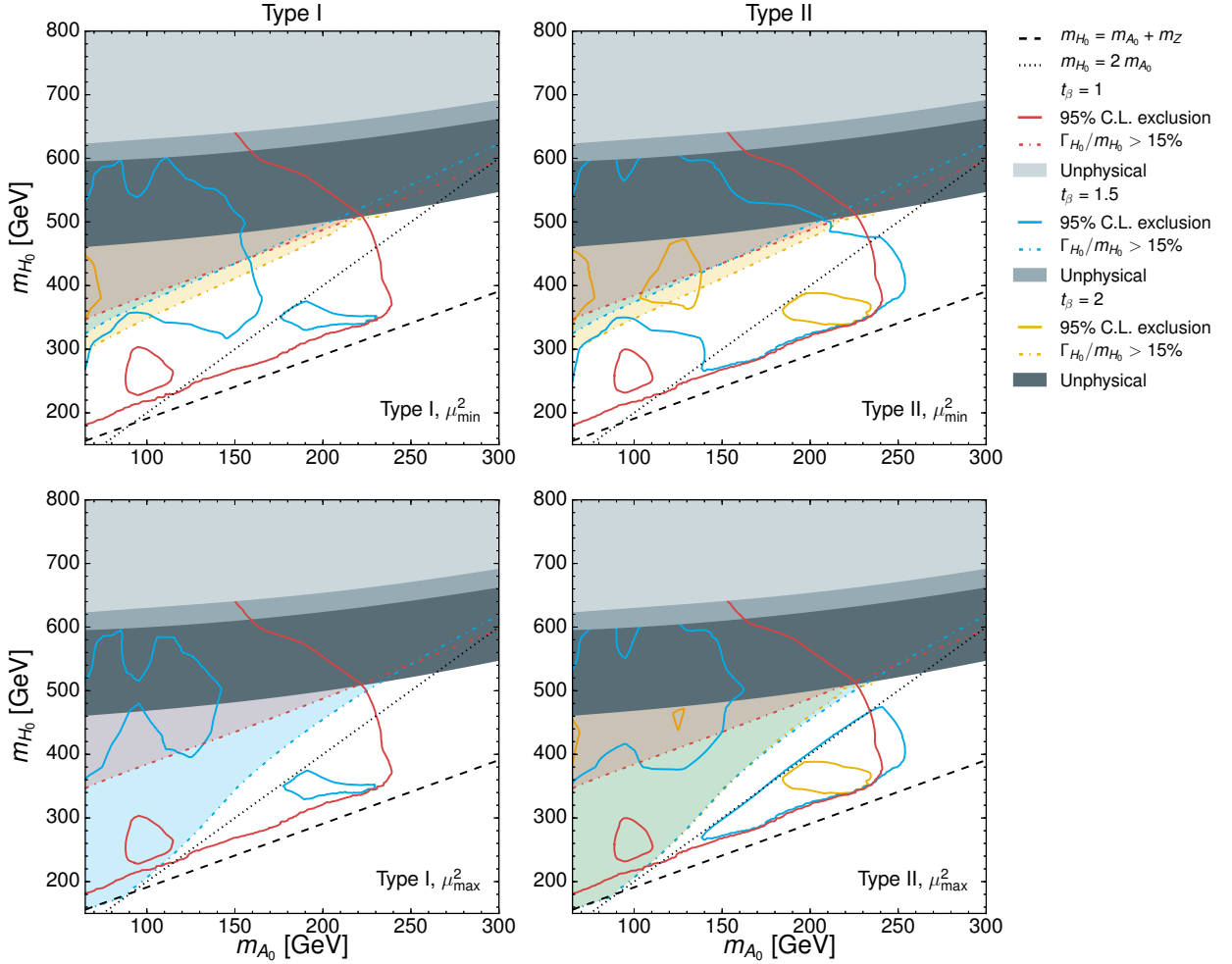


FIG. 9. Bounds on t_β in the (m_{A_0}, m_{H_0}) plane for $c_{\beta-\alpha} = 0$, from the search for $H_0 \rightarrow ZA_0 \rightarrow \ell\ell b\bar{b}$ performed in [20], For 2HDM of Type I (Left) and Type II (Right), and for $\mu^2 = \mu_{\min}^2/\mu^2 = \mu_{\max}^2$ (Top/Bottom respectively). The grey regions are theoretically excluded, while the shaded regions correspond to $\Gamma_{H_0}/m_{H_0} > 0.15$. The dotted-black line corresponds to $m_{H_0} = 2m_{A_0}$, above which the decay $H_0 \rightarrow A_0A_0$ becomes kinematically possible.

IV. HIERARCHICAL 2HDM AND LHC RUN II

LHC Run 2 at 13 TeV represents a great opportunity to dig further into the parameter space of hierarchical 2HDM scenarios, since the sensitivity of the searches described in the previous Section is limited mainly by small cross section values at the 8 TeV run of the LHC. While a detailed analysis of the LHC Run 2 prospects for the hierarchical scenario of the 2HDM is beyond the scope of this work, we present in this Section benchmark planes in (m_{A_0}, m_{H_0}) for $A_0 \rightarrow ZH_0$ searches, classified according to the 2HDM Type (I/II) and the proximity to the alignment limit. In Figure 10 (Top) we provide $\sigma(gg \rightarrow A_0 \rightarrow ZH_0) \times \text{BR}(H_0 \rightarrow X)$ for Type I/II (Left/Right) and a reference value $t_\beta = 3$, with X being the relevant decay mode of H_0 in each case: In alignment $c_{\beta-\alpha} = 0$ (Figure 10, Top), X is the main fermionic decay of H_0 , namely $b\bar{b}$ for $m_{H_0} < 340$ GeV and $t\bar{t}$ for

$m_{H_0} > 340$ GeV. Away from alignment $c_{\beta-\alpha} \gtrsim 0.2$ (Figure 10, Bottom), $X = W^+W^-$ and we choose $c_{\beta-\alpha} = 0.3$ for Type I, $c_{\beta-\alpha} = 0.5$ for Type II. We show in each case the constraint from the LHC Run 1 $A_0 \rightarrow ZH_0$ ($H \rightarrow b\bar{b}$) CMS search [20], noting that besides providing useful limits in alignment (recall Figure 6), it can also constrain the (m_{A_0}, m_{H_0}) plane away from alignment. This is most relevant in Type II, where $\kappa_d^{H_0}$ increases with t_β , and for $m_{H_0} \lesssim 180$ GeV as shown in Figure 10 (see also Figures 7 and 8). In contrast, for the benchmarks chosen away from alignment there are no limits from $gg \rightarrow H_0 \rightarrow W^+W^-$ searches in the whole (m_{A_0}, m_{H_0}) plane: for Type I this is due to $\kappa_u^{H_0} \ll 1$ (H_0 is approximately fermiophobic), while for Type II it is due to the $(\kappa_d^{H_0})^2$ enhancement of the partial width $\Gamma(H_0 \rightarrow b\bar{b})$ vs the $(\kappa_V^{H_0})^2$ suppression of the partial width $\Gamma(H_0 \rightarrow W^+W^-)$. The discussion above emphasizes the search $gg \rightarrow A_0 \rightarrow ZH_0$ ($H_0 \rightarrow W^+W^-$) as potentially key to probe a hierarchical 2HDM scenario away from the alignment limit.

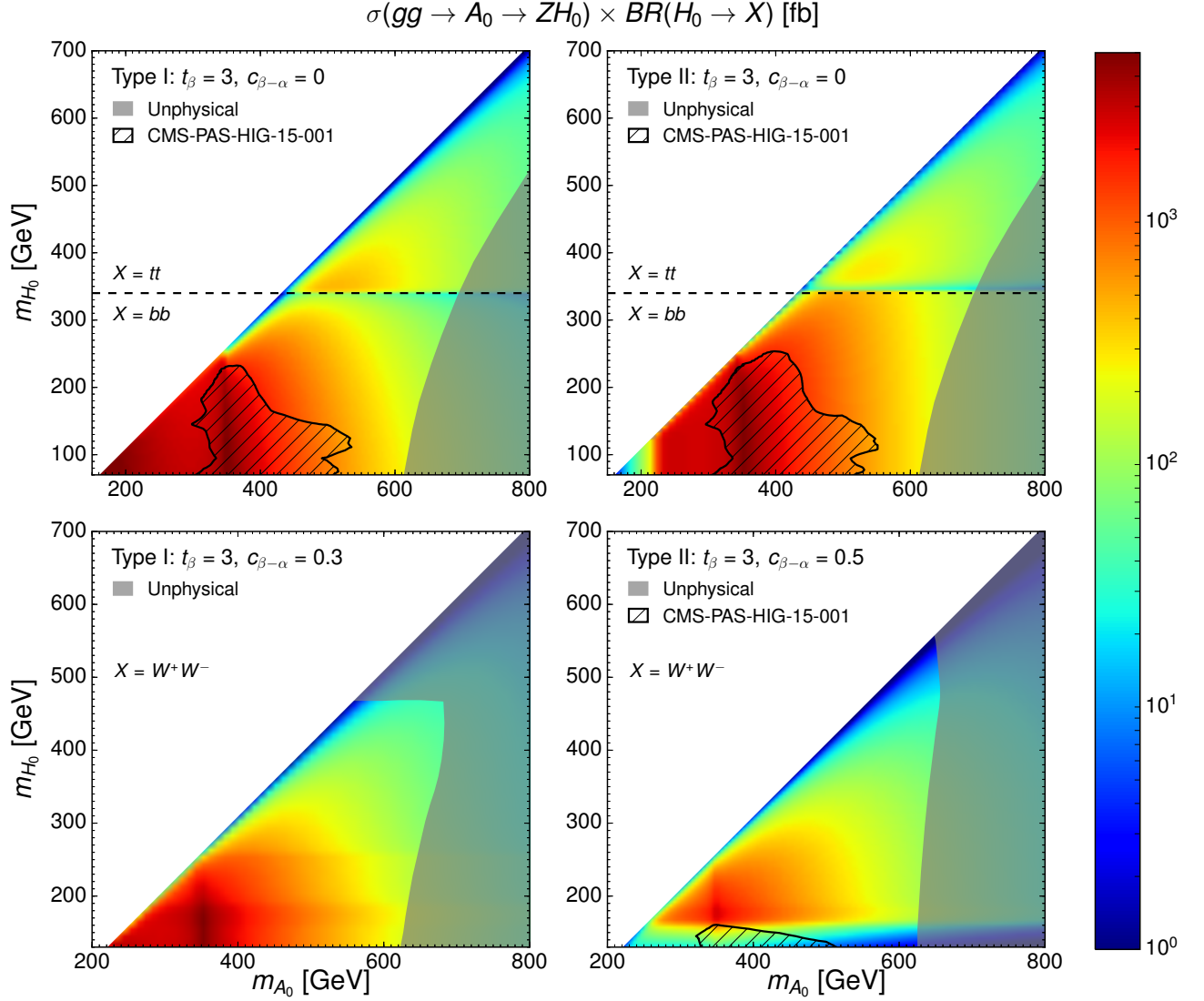


FIG. 10. Cross section $\sigma(gg \rightarrow A_0 \rightarrow ZH_0) \times BR(H_0 \rightarrow X)$ in the (m_{A_0}, m_{H_0}) plane, for Type I (Left) and Type II (Right). Top: Alignment limit $c_{\beta-\alpha} = 0$, with $X = \bar{b}b$ if $m_{H_0} < 340$ GeV and $X = t\bar{t}$ if $m_{H_0} > 340$ GeV. The dashed black region corresponds to the exclusion from the LHC Run 1 $A_0 \rightarrow ZH_0$ CMS search [20]. Bottom: Departure from alignment, with $X = W^+W^-$ and $c_{\beta-\alpha} = 0.3$ for Type I, $c_{\beta-\alpha} = 0.5$ for Type II. The value of the soft \mathbb{Z}_2 -breaking parameter is fixed to $\mu^2 = m_{H_0}^2 s_\beta c_\beta$ ($\Omega^2 = 0$, see discussion in Section III B). The grey regions are theoretically excluded.

Before concluding this section, a few comments are important: For Type II, the combination of Flavour bounds on m_{H^\pm} and EWPO would disfavour a 2HDM spectrum with both m_{A_0} and m_{H_0} significantly below 480 GeV, as discussed in Section III D. We choose not to show this in Figure 10, as these indirect limits (particularly the Flavour bound) could be modified in the presence of new physics. Also, while we do not discuss here the prospects for searches of H_0 decaying into non-SM states, we emphasize that searches for $H_0 \rightarrow ZA_0$ and $H_0 \rightarrow A_0A_0$ may be key to probe a hierarchical 2HDM scenario with $m_{H_0} > m_{A_0}$.

V. DISCUSSION AND OUTLOOK

Uncovering the full structure of the SM scalar sector and its possible extensions will be a central task for the LHC in the coming years. The results will have important implications not only for our understanding of the mechanism of electroweak symmetry-breaking but also for the origin of visible matter and the nature of dark matter. Extensions of the SM scalar sector that address one or both of these open questions may yield distinctive signatures at the LHC via modifications of the SM Higgs boson properties and/or the observation of new states.

In this work we have investigated the constraints on the parameter space of CP-conserving two-Higgs-doublet models of Types I/II in light of the ATLAS/CMS results from LHC Run 1. A key difference from the many similar analyses already existing in the literature is that the latter generally assume a nearly degenerate 2HDM spectrum for the new scalar states, which can then only decay into SM particles. While the properties of the observed 125 GeV Higgs are not affected by the mass spectrum of the new scalars (as discussed in Section III A), a large mass splitting between two or more of the new scalar states, *e.g.* $m_{A_0} - m_{H_0} \gtrsim m_Z$, causes new decay channels of the heavier scalars to open and become dominant. For such a *hierarchical* 2HDM, we show that the constraints usually obtained in the literature are *significantly* weakened. On the other hand, the new decay channels constitute novel ways of searching for these scalar states, *e.g.* $A_0 \rightarrow ZH_0$ and we show how they can be used to fill in the gaps left by previous analyses. We also highlight the importance of the μ^2 parameter, through its impact on the phenomenology of the heavier CP-even scalar H_0

and its sensitivity to unitarity and stability constraints.

Finally, we believe this analysis will strongly contribute to provide a global picture of the present status of 2HDMs in light of Run 1 LHC results, and of the prospects and relevant searches needed for exploring the still unconstrained regions of their parameter space.

Acknowledgements

We thank Jeremy Bernon for useful discussions. The work of S.H and K.M. is supported by the Science Technology and Facilities Council (STFC) under grant number ST/L000504/1. J.M.N. is supported by the People Programme (Marie curie Actions) of the European Union Seventh Framework Programme (FP7/2007-2013) under REA grant agreement PIEF-GA-2013-625809. G.C.D. is supported by the German Science Foundation (DFG) under the Collaborative Research Center (SFB) 676 Particles, Strings and the Early Universe.

-
- [1] G. Aad *et al.* [ATLAS Collaboration], arXiv:1507.04548 [hep-ex].
- [2] V. Khachatryan *et al.* [CMS Collaboration], Eur. Phys. J. C **75** (2015) 5, 212 doi:10.1140/epjc/s10052-015-3351-7 [arXiv:1412.8662 [hep-ex]].
- [3] G. C. Branco, P. M. Ferreira, L. Lavoura, M. N. Rebelo, M. Sher and J. P. Silva, Phys. Rept. **516**, 1 (2012) [arXiv:1106.0034 [hep-ph]].
- [4] J. M. Cline, K. Kainulainen and A. P. Vischer, Phys. Rev. D **54**, 2451 (1996) [hep-ph/9506284].
- [5] J. M. Cline and P. A. Lemieux, Phys. Rev. D **55**, 3873 (1997) [hep-ph/9609240].
- [6] L. Fromme, S. J. Huber and M. Seniuch, JHEP **0611**, 038 (2006) [hep-ph/0605242].
- [7] G. C. Dorsch, S. J. Huber and J. M. No, JHEP **1310** (2013) 029 [arXiv:1305.6610 [hep-ph]].
- [8] G. C. Dorsch, S. J. Huber, K. Mimasu and J. M. No, Phys. Rev. Lett. **113** (2014) 21, 211802 [arXiv:1405.5537 [hep-ph]].
- [9] G. Aad *et al.* [ATLAS Collaboration], arXiv:1509.00672 [hep-ex].
- [10] A. Celis, V. Ilisie and A. Pich, JHEP **1307**, 053 (2013) [arXiv:1302.4022 [hep-ph]].
- [11] M. Krawczyk, D. Sokolowska and B. Swiezewska, J. Phys. Conf. Ser. **447**, 012050 (2013) [arXiv:1303.7102 [hep-ph]].
- [12] B. Grinstein and P. Uttayarat, JHEP **1306**, 094 (2013) [Erratum-ibid. **1309**, 110 (2013)] [arXiv:1304.0028 [hep-ph]].
- [13] C. -Y. Chen, S. Dawson and M. Sher, Phys. Rev. D **88**, 015018 (2013) [arXiv:1305.1624 [hep-ph]].
- [14] N. Craig, J. Galloway and S. Thomas, arXiv:1305.2424 [hep-ph].
- [15] O. Eberhardt, U. Nierste and M. Wiebusch, JHEP **1307**, 118 (2013) [arXiv:1305.1649 [hep-ph]].
- [16] B. Dumont, J. F. Gunion, Y. Jiang and S. Kraml, Phys. Rev. D **90** (2014) 035021 [arXiv:1405.3584 [hep-ph]].
- [17] J. Bernon, B. Dumont and S. Kraml, Phys. Rev. D **90**, 071301 (2014) [arXiv:1409.1588 [hep-ph]].
- [18] N. Craig, F. D'Eramo, P. Draper, S. Thomas and H. Zhang, JHEP **1506**, 137 (2015) [arXiv:1504.04630 [hep-ph]].
- [19] J. Bernon, J. F. Gunion, H. E. Haber, Y. Jiang and S. Kraml, Phys. Rev. D **92**, no. 7, 075004 (2015) [arXiv:1507.00933 [hep-ph]].
- [20] CMS Collaboration [CMS Collaboration], CMS-PAS-HIG-15-001.
- [21] J. Bernon, J. F. Gunion, Y. Jiang and S. Kraml, Phys. Rev. D **91**, no. 7, 075019 (2015) [arXiv:1412.3385 [hep-ph]].
- [22] J. Bernon, J. F. Gunion, H. E. Haber, Y. Jiang and S. Kraml, arXiv:1511.03682 [hep-ph].
- [23] S. L. Glashow and S. Weinberg, Phys. Rev. D **15**, 1958 (1977).
- [24] M. Maniatis, A. von Manteuffel, O. Nachtmann and F. Nagel, Eur. Phys. J. C **48**, 805 (2006) [hep-ph/0605184].
- [25] B. Grinstein, C. W. Murphy and P. Uttayarat, arXiv:1512.04567 [hep-ph].
- [26] A. G. Akeroyd, A. Arhrib and E. M. Naimi, Phys. Lett. B **490**, 119 (2000) [hep-ph/0006035].
- [27] W. Grimus, L. Lavoura, O. M. Ogreid and P. Osland, J. Phys. G **35**, 075001 (2008) [arXiv:0711.4022 [hep-ph]].
- [28] B. Coleppa, F. Kling and S. Su, JHEP **1409**, 161 (2014) [arXiv:1404.1922 [hep-ph]].
- [29] B. Coleppa, F. Kling and S. Su, JHEP **1412**, 148 (2014) [arXiv:1408.4119 [hep-ph]].
- [30] T. Li and S. Su, arXiv:1504.04381 [hep-ph].
- [31] J. Bernon and B. Dumont, Eur. Phys. J. C **75**, no. 9, 440 (2015) [arXiv:1502.04138 [hep-ph]].
- [32] P. Bechtle, S. Heinemeyer, O. Stl, T. Stefaniak and G. Weiglein, Eur. Phys. J. C **74**, no. 2, 2711 (2014) [arXiv:1305.1933 [hep-ph]].
- [33] P. Bechtle, S. Heinemeyer, O. Stl, T. Stefaniak and G. Weiglein, JHEP **1411**, 039 (2014) [arXiv:1403.1582

- [hep-ph].
- [34] [ATLAS Collaboration], ATLAS-CONF-2013-030, ATLAS-COM-CONF-2013-028.
- [35] G. Aad *et al.* [ATLAS Collaboration], Phys. Lett. B **726**, 88 (2013) [Phys. Lett. B **734**, 406 (2014)] [arXiv:1307.1427 [hep-ex]].
- [36] The ATLAS collaboration [ATLAS Collaboration], ATLAS-CONF-2013-075.
- [37] S. Chatrchyan *et al.* [CMS Collaboration], JHEP **1401** (2014) 096 [arXiv:1312.1129 [hep-ex]].
- [38] CMS Collaboration [CMS Collaboration], CMS-PAS-HIG-13-017.
- [39] G. Aad *et al.* [ATLAS Collaboration], arXiv:1408.5191 [hep-ex].
- [40] S. Chatrchyan *et al.* [CMS Collaboration], Phys. Rev. D **89** (2014) 092007 [arXiv:1312.5353 [hep-ex]].
- [41] G. Aad *et al.* [ATLAS Collaboration], arXiv:1408.7084 [hep-ex].
- [42] V. Khachatryan *et al.* [CMS Collaboration], Eur. Phys. J. C **74** (2014) 10, 3076 [arXiv:1407.0558 [hep-ex]].
- [43] The ATLAS collaboration, ATLAS-CONF-2013-079, ATLAS-COM-CONF-2013-080.
- [44] S. Chatrchyan *et al.* [CMS Collaboration], Phys. Rev. D **89** (2014) 1, 012003 [arXiv:1310.3687 [hep-ex]].
- [45] The ATLAS collaboration, ATLAS-CONF-2013-108, ATLAS-COM-CONF-2013-095.
- [46] S. Chatrchyan *et al.* [CMS Collaboration], JHEP **1405** (2014) 104 [arXiv:1401.5041 [hep-ex]].
- [47] P. M. Ferreira, J. F. Gunion, H. E. Haber and R. Santos, Phys. Rev. D **89**, no. 11, 115003 (2014) [arXiv:1403.4736 [hep-ph]].
- [48] G. Aad *et al.* [ATLAS Collaboration], Phys. Lett. B **744** (2015) 163 [arXiv:1502.04478 [hep-ex]].
- [49] V. Khachatryan *et al.* [CMS Collaboration], Phys. Lett. B **748**, 221 (2015) [arXiv:1504.04710 [hep-ex]].
- [50] G. Aad *et al.* [ATLAS Collaboration], Phys. Rev. Lett. **113** (2014) 17, 171801 [arXiv:1407.6583 [hep-ex]].
- [51] CMS Collaboration [CMS Collaboration], CMS-PAS-HIG-14-006.
- [52] G. Aad *et al.* [ATLAS Collaboration], JHEP **1411** (2014) 056 [arXiv:1409.6064 [hep-ex]].
- [53] V. Khachatryan *et al.* [CMS Collaboration], JHEP **1410** (2014) 160 [arXiv:1408.3316 [hep-ex]].
- [54] [CMS Collaboration], arXiv:1307.7135.
- [55] R. V. Harlander, S. Liebler and H. Mantler, Computer Physics Communications **184**, 1605 (2013) [arXiv:1212.3249 [hep-ph]].
- [56] D. Eriksson, J. Rathsmann and O. Stal, Comput. Phys. Commun. **181**, 189 (2010) [arXiv:0902.0851 [hep-ph]].
- [57] [ATLAS Collaboration], ATLAS-CONF-2013-013, ATLAS-COM-CONF-2013-018.
- [58] G. Aad *et al.* [ATLAS Collaboration], arXiv:1412.2641 [hep-ex].
- [59] G. Aad *et al.* [ATLAS Collaboration], Phys. Rev. Lett. **114** (2015) 8, 081802 [arXiv:1406.5053 [hep-ex]].
- [60] V. Khachatryan *et al.* [CMS Collaboration], arXiv:1504.00936 [hep-ex].
- [61] CMS Collaboration [CMS Collaboration], CMS-PAS-HIG-13-032.
- [62] V. Khachatryan *et al.* [CMS Collaboration], arXiv:1503.04114 [hep-ex].
- [63] M. Misiak *et al.*, Phys. Rev. Lett. **114** (2015) 22, 221801 [arXiv:1503.01789 [hep-ph]].
- [64] T. Hermann, M. Misiak and M. Steinhauser, JHEP **1211** (2012) 036 [arXiv:1208.2788 [hep-ph]].
- [65] The ATLAS collaboration [ATLAS Collaboration], ATLAS-CONF-2013-090.
- [66] G. Aad *et al.* [ATLAS Collaboration], JHEP **1503**, 088 (2015) [arXiv:1412.6663 [hep-ex]].